Feedback control of organ size precision is mediated by *BMP2*-regulated apoptosis in the *Drosophila* eye

T. Navarro1, A. Iannini1, M. Neto1,5, A. Campoy1,2, Javier Muñoz3, S. Ares4*, F. Casares 1*
1 – CABD, CSIC/Universidad Pablo de Olavide. 41013 Seville, SPAIN.
2 – ALMIA, CABD, CSIC/Universidad Pablo de Olavide. 41013 Seville, SPAIN.
3 – Universidad Carlos III, 28911 Madrid, SPAIN.
4 – CNB, CSIC/UAM, 28049 Madrid, SPAIN.
5 – Present address: Instituto de Neurociencia, CSIC/Universidad Miguel Hernandez, 03550 Sant Joan d'Alacant, SPAIN.
* Corresponding authors: fcasfer@upo.es; saul.ares@csic.es

SUMMARY

Biological processes are intrinsically noisy and yet, the result of development –like the species-specific size and shape of organs– is usually remarkably precise. This precision suggests the existence of mechanisms of feedback control that ensure that deviations from a target size are minimized. Still, we have very limited understanding of how these mechanisms operate. Here, we investigate the problem of organ size precision using the *Drosophila* eye. The size of the adult eye depends on the rates at which eye progenitor cells grow and differentiate. We first find that the progenitor net growth rate results from the balance between their proliferation and apoptosis, with this latter contributing to determining both final eye size and its variability. In turn, apoptosis of progenitor cells is hampered by Dpp, a BMP2/4 signaling molecule transiently produced by early differentiating retinal cells. Our genetic and computational experiments show how the status of retinal differentiation is communicated to progenitors through the differentiation-dependent production of Dpp which, by adjusting the rate of apoptosis, exerts a feedback control over the net growth of progenitors to reduce final eye size variability.

INTRODUCTION

The size of some organs is remarkably precise (Boulan and Leopold, 2021). Although this precision is a functional need, it is not easily explained (Lander, 2011; Wolpert, 2010). Most organs are specified as small primordia whose growth is exponential. However, exponential growth is prone to amplify the noise that is inescapable to biological processes. This fact has led to the proposal that organ development must be subject to mechanisms of feedback control (Lander, 2011) which, in the engineering sense, reduce their internal "developmental instability" (Waddington, 1942) and increase the precision with which organs reach their species-specific size. Some organs that undergo constant tissue renewal, like the mammalian olfactory epithelium, maintain their size homeostasis through integral feedback (Lander et al., 2009). Some other organs, though, grow to a size that, once reached, cannot be further modulated. This is the case of insects. After their last molt, the adult organs cease growth and then become covered in a rigid chitin exoskeleton that precludes further size regulation. The eye of *Drosophila* fruitflies serves as a good example of this type of organ growth: In *Drosophila,* the end point of eye development is reached when all retinal progenitor

cells differentiate, as differentiation is accompanied by the exit of the cell cycle. Three features should have resulted in a strong evolutionary pressure to maximize the precision in eye size: first, size impacts vision directly, as image resolution and contrast sensitivity is proportional to the number of light sensing units in the eye (Casares and McGregor, 2020); second, making and maintaining the eyes is energetically very expensive (Niven and Laughlin, 2008) so there is a need to match eye size to vision needs; and third, left and right eyes must survey a symmetrical part of the space, so eye asymmetry, which could be driven by developmental noise, should be minimized. In this paper we investigate the mechanism by which the *Drosophila* eye ensures its size precision as an example of organ size control.

The development of the *Drosophila* eye takes place as a wave of differentiation crosses the eye primordium during the last larval stage (Figure 1a,b). As the wave moves, proliferative progenitors anterior to the wave are recruited as differentiating retinal cells that exit the cell cycle. Final eye size is attained when the differentiation wave reaches the anterior-most region of the primordium: with no remaining progenitors, which are the source of growth, the process ends. The movement of the wave is driven primarily by two secreted signaling molecules. The first of them is Hh (*hedgehog*). Hh's major role is the induction of differentiation of progenitor ("G") cell into retinal ("R") cells (Heberlein and Moses, 1995), a role that is shared by its homologue Shh in the differentiation of the ganglion cells of the vertebrate retina (Neumann and Nuesslein-Volhard, 2000). Hh, initially expressed adjacent to the eye primordium, contributes to initiate R differentiation. Once initiated, R cells produce Hh themselves (Lee et al., 1992; Ma et al., 1993), resulting in the self-sustained progression of a differentiation wave (Rogers et al., 2005). The second signal is a BMP2/4 homologue, Dpp (*decapentaplegic*). *dpp* expression is induced by Hh in the newly-recruited retinal cells ("Rn") (Chanut and Heberlein, 1995; Heberlein et al., 1993). Dpp, by repressing the progenitor transcription factor Hth (*homothorax*) increases the propensity of progenitors to enter differentiation (Bessa et al., 2002; Lopes and Casares, 2010). However, and in contrast with Hh, whose expression is maintained in differentiated R cells, Dpp is expressed only transiently: as newly recruited Rn cells progress along their differentiation to Rs, *dpp* expression is turned-off (Blackman et al., 1991; Heberlein et al., 1993; Masucci et al., 1990). Thus, a stripe of Dpp marks the front of the differentiation wave (Figure1a). This process is schematically represented in Figure 1c.

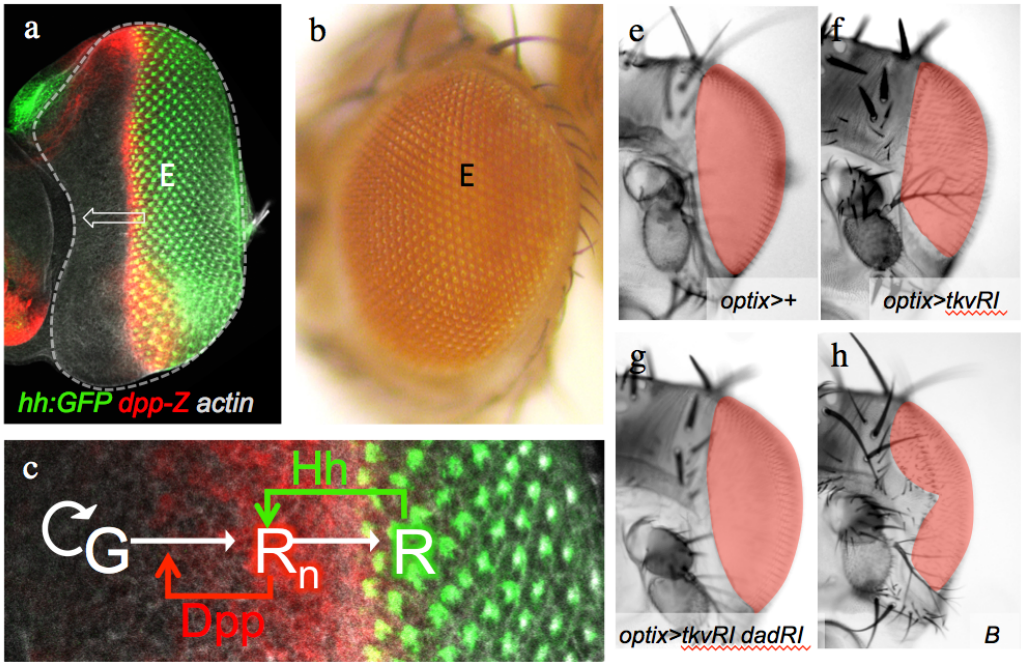

Figure 1. The eye primordium ((a) "E", outlined) develops into the adult eye (b) through the action of a differentiation wave that sweeps across it (arrow). (a) eye primordium ("E") of a *Hh:GFP*; *dpp-Z* larva. The differentiation wavefront expresses *dpp-Z.* Posterior to it further differentiated photoreceptors lose *dpp* expression and express Hh. (b) Lateral view of an adult *Drosophila* eye. (c) The recruitment of proliferative progenitor cells ("G") into early differentiating (*dpp*-expressing) retinal cells ("Rn") and then into terminally differentiating (non-*dpp*-expressing) retinal cells ("R") is controlled by two signaling molecules, Hh and Dpp. (e-h) Frontal views of female heads of the indicated genotypes, with the eyes colored for better visualization. (e) Control, *optix>+,* (f) *optix>tkvRNAi,* (g) *optix>tkvRNAi + dadRNAi,* (h) *Bar (B) mutant*. See main text for details.

RESULTS

To ensure that the target, species-specific final size is reached with precision, the rates of growth and of differentiation need to be coordinated within the eye primordium (Casares and McGregor, 2020; Fried et al., 2016; Lobo-Cabrera et al., 2021). For example, a transient halt of the differentiation wave would produce some excess of progenitor cells and a concomitant deviation from the target size -unless this halt were communicated to the progenitors as a negative feedback on their rate of growth. This feedback could be implemented either by slowing down progenitor proliferation or by curving the excess of progenitor cells through cell death (we do not consider a change in cell size as this change would alter the size of the ommatidia and thus their optical properties). We noticed that, in wild-type control eye primordia, the apoptosis signal detected using an antibody against the activated form of caspase-3 is usually very low. However, if an antibody against the terminal caspase Dcp-1 (Song et al., 1997) is used instead, we detected a stripe of apoptotic cells just anterior to the differentiation wave-front (Suppl. Fig1. to Fig. 1). Likely, the activation of cas-3 is more brief than the expression of dcp-1 during the apoptotic process, making detection of apoptosis easier with Dcp-1 as a marker.

In any case, we were intrigued by this localized apoptosis happening in normal eye primordia and asked what its role could be. To answer this, we blocked apoptosis by driving, specifically anterior to the differentiation wave-front, a polycistronic RNAi against *reaper, hid* and *grim*, the three major pro-apoptotic genes in *Drosophila* (*optix>Reaper,Hid,Grim-RNAi,* abbreviated *optix>RHGRI* (Siegrist et al., 2010)). These flies showed two major phenotypic changes: first, the median eye size ("rE" = average intraindividual eye area relative to head area expressed as percentage) was larger than those of controls (*optix>+)* and, second, the distribution of eye sizes was also significantly broader (Figure 2a and Supp. table 1 to Figure 2). When we measured the apoptotic index of *optix>RHGRI* it was smaller than that of *optix>+* and very close to zero (Figure 3). The increased dispersion in the distribution of eye size is indicative of a loss in size precision. The fluctuating asymmetry index (FAi), which measures the disparity between left and right organs within the same individual, has also been frequently used as a measure of precision as it captures the sensitivity of the process to developmental noise (Parsons, 1992). The FAi is normally calculated as the absolute value of the normalized difference between the size of the left (L) and right (R) organs from the same individual. Here, we use the *signed* FAi ("sFAi") to have into account the sign of the asymmetry, $(L-R)/(L+R)$, which allows to compare the asymmetry across different genotypes based on the amplitude of the distribution of this metric for each of them (Figure 2b and Suppl. table 1 to Figure 2). In apoptosis-blocked individuals the variance of sFAi increased significantly as well. To control for potential non-specific effects on eye size and its variability of RNAi overexpression, we drove a "neutral" RNAi against the fluorescent protein Cherry (*optix>CherryRI*) and observed that it did not affect neither of the two parameters when compared to control (*optix>+*) or wild type (*Oregon-R*) flies (see Suppl. Fig. 1 to Figure 2).

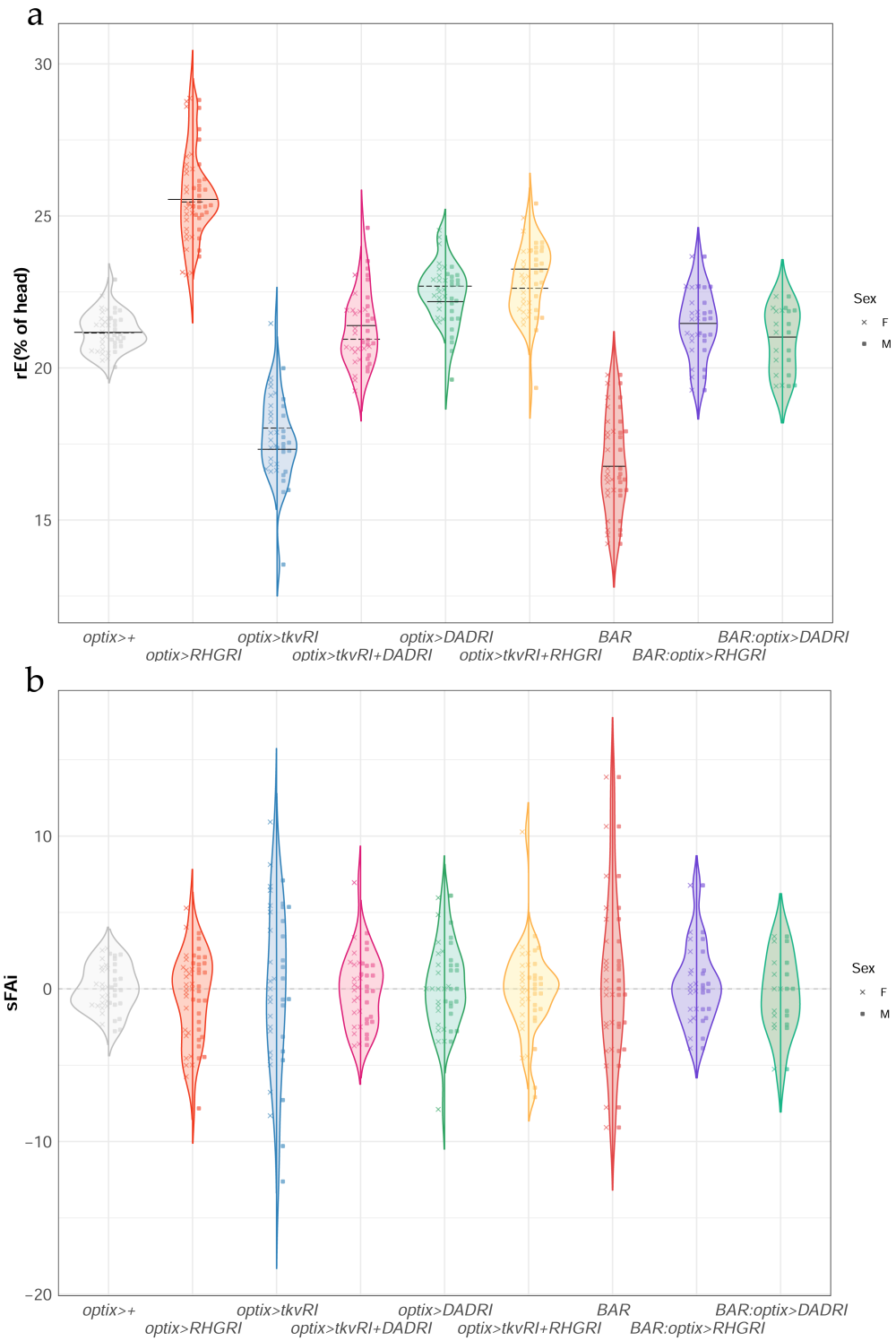

Figure 2. Effects of different genetic manipulations on the distribution of eye size ("rE") (a) and signed Fluctuating Asymmetry index ("sFAi", b). Each violin plot includes the male (left) and female (right) distributions, which were not significantly different from each other in any genotype. The median of each distribution is indicated (solid and dashed line, male and female, respectively). The predicted rE median for each genotype and the statistical model from which they are derived can be found in Suppl. Table 1 to Figure2. The variances of each genotype were compared against the variance in the control group (*optix>+)* in rE and sFAi (Suppl. table_1 to Figure2). Eye area is measured relative to the total head area and expressed as a percentage in this and subsequent figures.

These results pointed to a role of developmental apoptosis in controlling eye size and its precision. But in order to be involved in such control, the apoptotic rate in progenitors should be coupled to the rate of eye differentiation. This communication between progenitors and differentiating cells might be exerted by either of the two major signals in eye development: Hh and Dpp.

Intuitively, if one of these two signals were to be used to convey feedback information to progenitors about the status of retinal differentiation, Dpp would seem a better candidate. Although both Hh and Dpp regulate progenitor gene expression (Greenwood and Struhl, 1999), Dpp, by being expressed transiently, can be better used as readout of the *rate* of retinal differentiation. In contrast, Hh is constantly produced in R cells, regardless of whether the wave is moving or not. If Dpp were used in a feedback control mechanism, it would be expected that the attenuation of its signaling pathway in progenitors should lead to a decrease in final eye size precision. In addition, prior work on *dpp* mutant alleles had shown an increase in apoptosis in the mutant eye primordia (Bryant, 1988; Masucci et al., 1990), reinforcing the idea that Dpp could be this coupling signal.

To test this point, we attenuated the Dpp pathway specifically in eye progenitors during development, by targeting the expression of an RNAi against the Dpp receptor *tkv* (*thickveins*) (Brummel et al., 1994) in these cells (*optix>tkvRI*). This treatment caused two effects: First, the median eye size was reduced (Figures 1e,f and 2a and Suppl. table1 to Figure 2). This effect -eye reduction- had been described previously for mutant alleles of *dpp* (Spencer et al., 1982) and explained as a consequence of Dpp's requirement in progenitor cell recruitment (Chanut and Heberlein, 1997; Greenwood and Struhl, 1999). The eye size reduction was concomitant to a dramatic increase of both the dispersion of the eye size distribution and of its sFAi (Figure 2b and Suppl. table1 to Figure 2), something expected if Dpp were involved in feedback control. To confirm that this phenotype resulted from the attenuation of the Dpp pathway, we simultaneously drove expression of RNAis against *tkv* and against *dad* (*daughters against-dpp*), a Smad molecule that acts as a feedback inhibitor of the pathway (Inoue et al., 1998; Tsuneizumi et al., 1997). In individuals of this genotype (*optix>tkvRI+DadRI*) the eyes almost recovered their control size (Figure 1e,f and 2a, Suppl. table1 to Figure 2). Similarly, the dispersion of eye size distribution as well as the sFAi decreased towards values closer to control, although not fully (Figure 2b, Suppl. table1 to Figure 2). The attenuation of the *tkv-RNAi* effect cannot be attributed to its weaker expression caused by the introduction of a second UAS sequence (*UAS-Dad-RNAi*) in the genotype (Suppl. Fig. 2 to Figure 2).

Next, we confirmed that attenuation of the Dpp pathway (*optix>tkvRI*) caused a dramatic quantitative increase in dcp-1 apoptotic signal (Figure 3 and Suppl. Table 1 to Figure 3), while the mitotic rate of progenitors remained unaffected (Suppl. Fig. 1 to Figure 3), and that this increase in apoptosis was rescued by coexpression of the Dad-RNAi (*optix>tkvRI+DadRI*) (Figure 3). The expression of *UAS-RHGRI* alone or in combination resulted in the reduction of apoptosis almost completely (Figure 3).

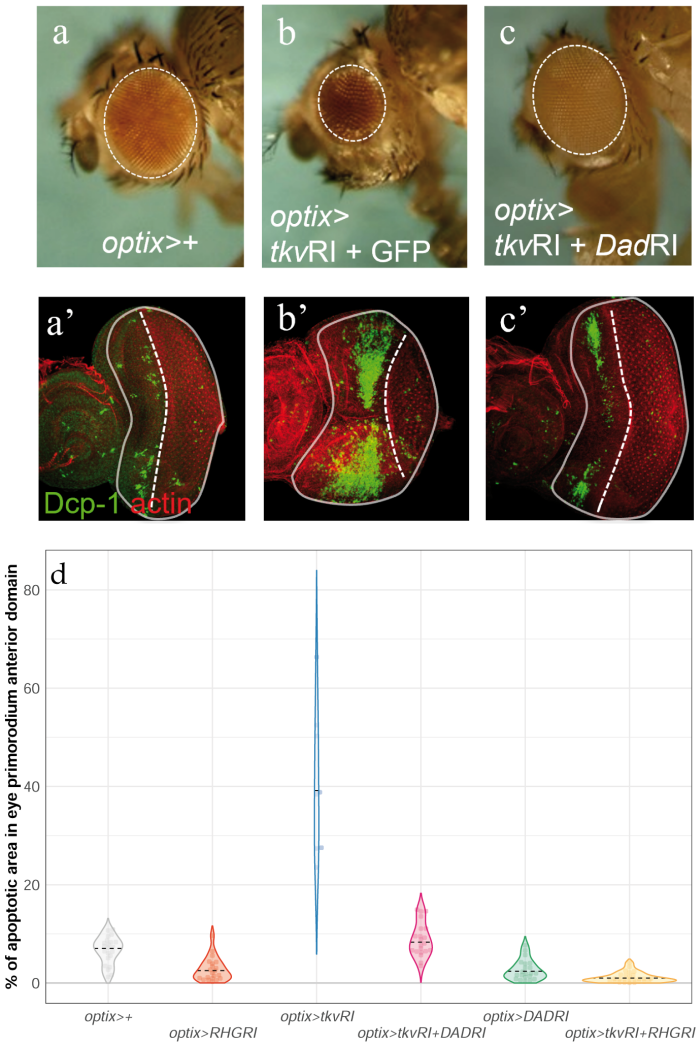

Figure 3. Eye size reduction and apoptosis induced by attenuation of the Dpp signaling pathway can be reverted by blocking Dad. Lateral views of adult eyes (a-c) and L3 eye discs, stained with Dcp-1 (and counterstained with rhodamine phalloidin, "actin") (a'-c') of the indicated genotypes. (d) Distribution of apoptosis intensity in L3 discs of the indicated genotypes. Blocking apoptosis driving the UAS-RHG-RNAi reduces the apoptosis caused by *tkv* attenuation (*optix>tkvRI + RHGRI*). The statistical analysis corresponding to these data can be found in Suppl. Table 1 to Figure 3.

Therefore, we expected that any perturbation affecting the coupling between retina and progenitor apoptosis would not be able to fully rescue the size precision observed in control flies (both the dispersion of the eye size distribution or the sFAi). This was the case in all the experiments in which the feedback between retina-produced Dpp and apoptosis was disrupted, either by artificially upregulating the Dpp pathway (expressing *dad-RNAi*) or by blocking apoptosis (expressing the RHG-RNAi) (Figures 2a,b and Suppl. table 1 to Figure 2).

To further substantiate our results, we decided to analyze the phenomenon of eye size control in another mutant situation in which the *dpp* pathway was affected. We chose the *Bar ("bar-eyed")* mutant. *Bar*-mutant eyes are reduced (Tice, 1914)(Figure 1e,h)

212 and this size reduction is associated with the control of *dpp* expression and an
213 increased apoptosis during larval development (Kang et al., 2014). In *Bar* eye
214 primordia we detected a fragmented *dpp* expression, monitored by the *dpp-Z*
215 transcriptional reporter, and an increased dcp-1-positive apoptosis (Figure 4a,b).
216
217 **Figure 4. Increased cell death and fragmented *dpp* expression in *Bar* discs.** L3 *dpp-Z*
218 discs (a,b), stained for apoptosis (dcp-1, green), *dpp* transcription (beta-galactosidase, red) and
219 the retinal differentiation marker Elav (blue). (a) control ("+": Oregon-R) and (b) *Bar* mutant
220 discs. The ellipse approximately outlines the eye region. "*a*" marks the antennal primordium.

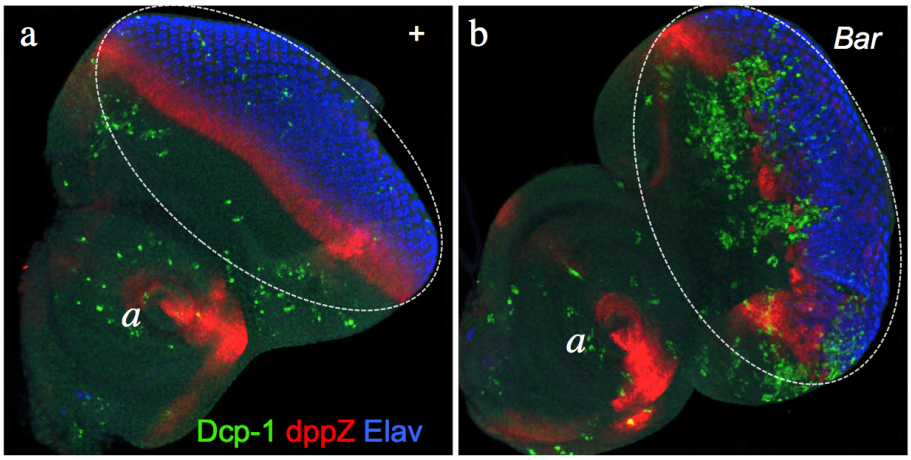

221
222
223 *Bar* eyes are smaller and more variable (Figure 2a) as well as more asymmetric
224 (Figure 2b) than control flies (see also Suppl. table 1 to Figure 2). Similarly to what
225 happened in our previous experiments, in which the Dpp pathway was attenuated
226 directly by targeting the Dpp receptor with an RNAi, either blocking apoptosis (*Bar;*
227 *optix>RHGRI*) or derepressing the Dpp pathway (*Bar; optix>DadRI*) partly rescued eye
228 size (Figure 2a) and reduced both eye dispersion (Figure 2a) and their fluctuating
229 asymmetry (Figure 2b; Suppl. table 1 to Figure 2).
230
231 The results obtained so far indicated that a major role of Dpp during eye development
232 was the regulation of developmental apoptosis. Losing this regulation, by either
233 blocking apoptosis directly or by "disconnecting" retina and progenitors by the
234 attenuation of Dpp signal (by *tkvRI* expression or in *Bar* mutants), led to a decreased
235 size precision. Therefore, not only the size of the eye, but its precision is under the
236 control of the Dpp pathway.
237
238 The fact that the effects on eye size and precision caused by *dpp* signaling attenuation
239 were almost fully rescued by preventing apoptosis pointed to the regulation of this
240 process as a key phenomenon. In order to explore further how the regulation of
241 apoptosis impinges on eye size, we built and analyzed a mathematical model of the
242 process. With this model, we first explored whether our description of the biological
243 phenomenon is complete by testing if the model recapitulates the biological results
244 when parameterized using experimental measurements.
245 Our model comprises G (progenitors), Rn (newly differentiated retinal cells, expressing
246 *dpp*) and R (differentiating retinal cells, no longer expressing *dpp* but producing Hh)
247 cells as variables, as well as their transformations: proliferation of progenitors ("self-

renewal": G → G + G), apoptosis of progenitors (G → Φ), initial differentiation of progenitors into *dpp*-expressing early retinal cells (G → Rn) and final differentiation of these cells into *hh*-expressing photoreceptors (Rn → R) (Figure 5a,b), and includes noise in all four differentiation steps. Its full description is available as Supplementary material.

Conceptually, our model expresses the rates at which the G, Rn and R cells change over time as in Figure 5c, where the variables influencing each of the steps (e.g. "proliferation") are within the parentheses (e.g. "G, Rn").

Figure 5. Overview of the model of the G→Rn→R including apoptosis (Φ). (a) Schematics of the process. R cells stimulate the differentiation process (by expressing Hh). Rn cells negatively regulate apoptosis (by producing Dpp). G cells can divide, die or progress further into differentiation by transiting to Rn. (b) This process, schematized in space. MF: morphogenetic furrow, is the differentiation wavefront that moves (arrow) from posterior (right) to anterior (left). L_A, L_P are the maximum distances anterior and posterior to the MF, respectively. The L_p can be used as a proxy for developmental time: as the MF moves with constant speed, L_p increases as time passes. L_A corresponds to G cells. L_p comprises Rn (orange bar) + R cells. (c) "Qualitative" model. (d) Typical temporal profiles of all populations as predicted by the model. (e) The model fits experimental data (L_{AP} as minor axis of elliptical fits of eye primordia (blue points) and $L_A = L_{AP} - L_p$ (orange points)) very well (see main text and supplementary material for details).

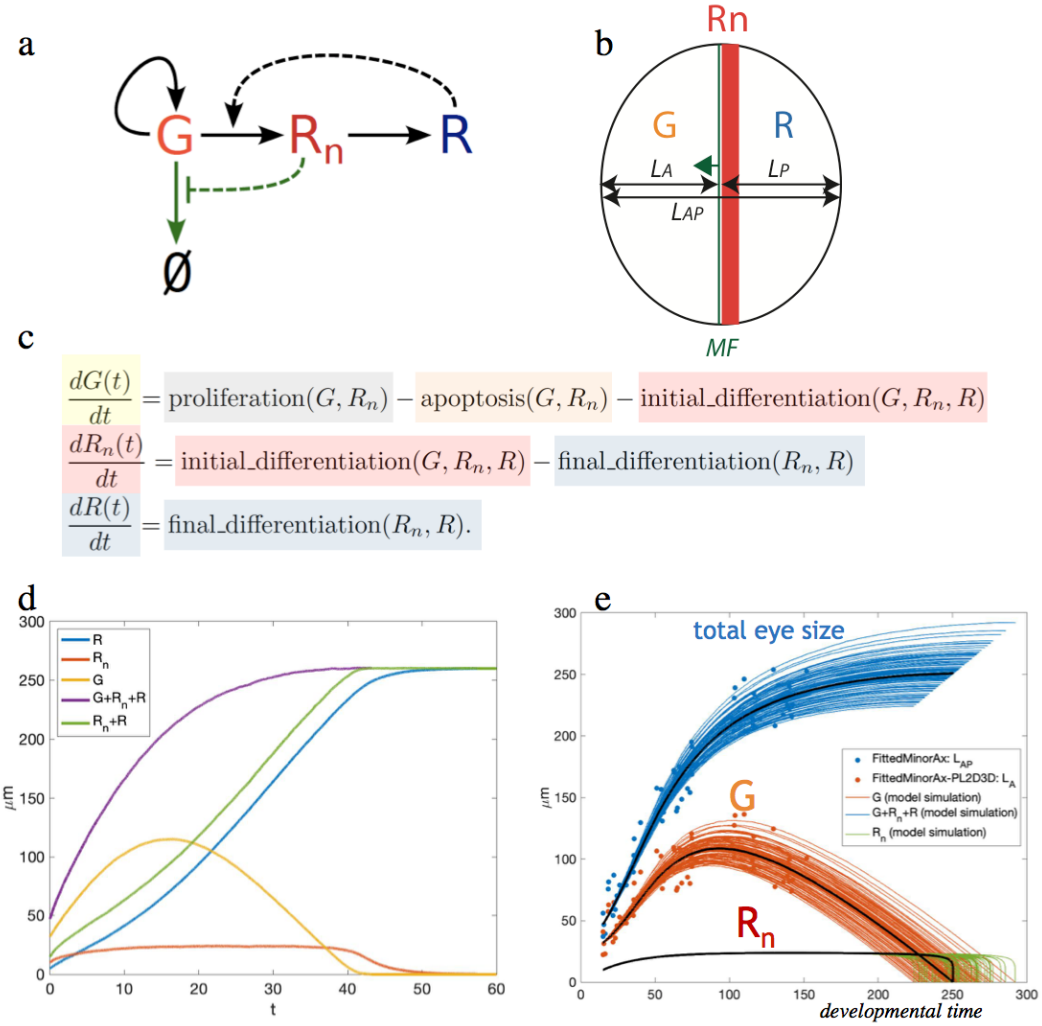

The key processes are modeled as follows: apoptosis is a decreasing function of the

Dpp-producing Rn cells, because the more Dpp the less apoptosis, and is proportional to the number of progenitors (G), such that $apoptosis = a(Rn)G$. All G cells not entering apoptosis will be proliferating with $proliferation = 1 - a(Rn)G$. As for the rate of G to Rn differentiation ("early differentiation") we have considered two factors. First, the activation of differentiation would depend on an increasing function of the Hh-producing R cells, $h(R)$. Second, the induction of G cells to differentiate is limited to the range of action of Dpp produced by Rn. Therefore, since beyond a certain point having more G cells will not result in increased differentiation (that is, those G cells out of the range of action of the signals will not be recruited), we modeled the function describing G growth as a saturating sigmoidal function $f(G)$. Imposing $f(0) = 0$, this function also ensures that once the G population has been exhausted, no further differentiation can occur. Thus, $initial\ differentiation = f(G)h(R)$. Finally, the final differentiation, or transition from Rn into R, can be expressed as being proportional to Rn, as in $final\ differentiation = b * h(R)Rn$, where *b* is a constant. With this expression we indicate that *Rn* differentiates "automatically" into R cells with a constant pace, simplifying a complex process of successive cell induction leading to the formation of the ommatidial cell types (Roignant and Treisman, 2009). However, eye size does not depend on this process, as the number of ommatidia and therefore, the size of the eye, is directly related to the number of G cells that are recruited as Rn cells. The expressions of the relevant functions $a(Rn), f(G)$ and $h(R)$ can be found in the full description on the model in the supplementary material. These functions allow us to model the RNAi treatments as well.

With this model, we can calculate the evolution of all these cell populations over time (Figure 5d). First, we fitted the model to an experimentally determined growth curve of the eye primordium (Figure 5e; data from (Vollmer et al., 2016)). Since the differentiation velocity is about constant during most of development (Vollmer et al., 2016; Wartlick et al., 2014) the width of the R + Rn domain (the distance between the posterior margin of the primordium to the differentiation wave-front, called "posterior length", or "Lp") is a proxy for elapsed developmental time, and we used it as a time axis (as in (Vollmer et al., 2016)). The fitting demanded that the growth rate of G cells declined over developmental time, something that had been shown experimentally (Vollmer et al., 2017; Wartlick et al., 2014). With these parameters, the fitting of the model to the data was very good, indicating that the model captured the biology underneath the control of eye size and its variability (Figure 5e and Suppl. Fig. 1 to Figure 5).

Since the model was able to recapitulate well the dynamics of eye differentiation, we asked which conditions would allow the system to reach robustly a final size. This can be done by carrying out a linear stability analysis of the system. The "set point" that needs to be stable is the final eye size, R*. Note that this analysis says nothing about what the actual final eye size R* is (this depends on the specific rates and initial conditions), just how stable it is. The finalization of the process is attained when G=0 and Rn=0: without any G and Rn cells left, the eye has reached R*. This R* state is unstable, though. Any fluctuation (noise) in the number of G or Rn cells would alter the value of R*. However, the linear stability analysis (see Linear stability analysis of the deterministic model in supplementary materials) indicates that there is a factor that

strongly favors stability: the "basal apoptotic probability", a_0, which is the G cells' tendency to enter apoptosis in the absence of Dpp signaling, with high apoptotic rates favoring stability, since apoptosis promotes the depletion of the G pool and therefore the termination of growth. Specifically, with an a_0 = 0,4 (i.e. 40% of apoptosis determined experimentally in *optix>tkvRI*), this apoptosis rate would be close to ensuring the R* stability condition on its own (see supplementary Linear stability analysis). Therefore, high propensity of apoptosis in progenitor G cells seems to be a requirement for robust size. Next, we used our model to predict the effects that noise would have on eye size in different genotypes with different rates of apoptosis.

We reasoned at the onset that regulating organ size would rely on the differentiating retina feeding information about its status on progenitor growth rates (something we have shown to occur through the modulation of apoptosis). Therefore, we simulated the effects of increasing the noise in the recruitment of Rn cells ("initial differentiation"), which are the source of Dpp, on eye size and its variation in three genotypes: two in which apoptosis is possible (control (*optix>+*) and *dpp* signaling attenuated (*optix> tkv-RNAi*)) and one in which apoptosis is blocked (*optix>RHG-RNAi*) (Figure 6). While increasing noise in Rn affects very little the MEDIAN eye size in the two genotypes where apoptosis is allowed, it results in a steady increase of eye size if apoptosis is blocked (until the noise levels are very high, when allowing apoptosis or not becomes irrelevant). This computational result reinforces the idea that the *dpp*-sensitive apoptosis of progenitors is instrumental in maintaining the developmental stability of eye size.

Figure 6. Effects of increasing noise strength on median eye size (rE). If apoptosis is blocked (by setting to zero the apoptotic rate of progenitors in the computational model, equivalent to *optix>RHG-RI*) eye size increases more rapidly than in the other two genotypes, in which apoptosis is allowed, until noise is too high (beyond 10^2), point at which allowing apoptosis or not becomes irrelevant. Computational results. Data for each point is from 200 simulations *per* genotype.

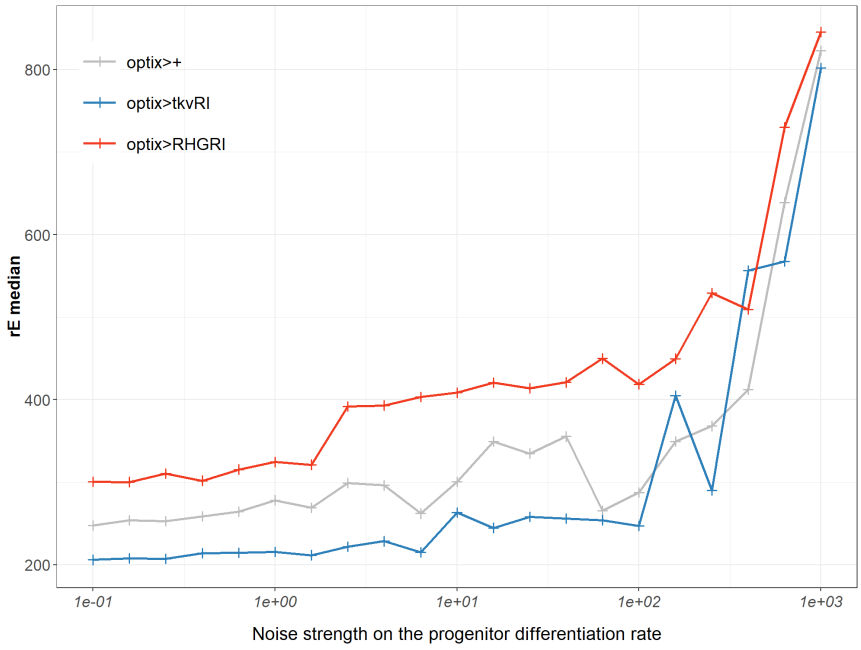

DISCUSSION

For organs to attain a final size with low variability, mechanisms of control must exist to reduce the effects of developmental noise. In this paper, we describe one such mechanism, in which the processes of eye growth and differentiation are coupled through a feedback control. In this feedback, the discrepancies between the rates of growth and differentiation of progenitors are adjusted through the modulation of the progenitor cells' propensity to enter apoptosis, so that any production of progenitors in excess is curved, as a proportion of these progenitors will not receive sufficient Dpp signaling to overcome apoptosis. In this way, it is the Dpp production which, acting as a surrogate of the process of differentiation, feeds back onto the growth rate of progenitors, a rate that depends on their combined proliferation and apoptosis (this latter Dpp-signaling dependent). When analyzing our data, comparing the actual FAi versus the fluctuating asymmetry of randomized pairs generated from the same experimental data (FAn), we observed that FAn was slightly larger than FAi, and this difference (FAn>FAi) was invariant across genotypes. This indicated a small, but consistent effect of the individual. Therefore, although most variation in size can be attributed to organ-autonomous variation, the two eyes from an individual are slightly correlated (Suppl. Fig. 3 to Figure 2). This is expected though, as it has been shown that, besides organ-autonomous mechanisms of growth control, the growth discrepancies among organs in an individual affect the systemic growth of the organism through neuroendocrine communication mediated by insulin-like peptides (Colombani et al., 2012; Garelli et al., 2012). In addition, each larva might be exposed to small microenvironmental variations during its growth (Morgante et al., 2015). Still, our results indicate that the feedback mechanism we have described operates mostly in an organ-autonomous manner.

Our experiments show that a major role of *dpp* signaling during eye development is the regulation of apoptosis, since the effects on eye size caused by attenuating this pathway are almost fully recovered just by blocking it. This role is very different from the function in cell differentiation that has normally been attributed to *dpp* during eye development (Chanut and Heberlein, 1997). We note, however, that in our experiments, by using RNAi, we are attenuating, rather than fully abrogating, *dpp* signaling. This could mean that the low levels of signaling presumably remaining could still participate in cell fate specification. This would be similar to the situation found in the wing disc, with different signaling thresholds being important for distinct functions, with high *dpp* signaling being necessary for wing patterning, while lower levels sufficing for tissue growth (Barrio and Milan, 2017; Bosch et al., 2017; Matsuda and Affolter, 2017). Recently, the Kumar laboratory has shown that the main role of the Pax6 gene *eyeless (ey)*, a gene essential for normal eye development (Hunt, 1971), is the activation of *dpp* transcription (Weasner and Kumar, 2022). Interestingly, loss of *ey* function causes abundant cell death in eye progenitors (Zhu et al., 2017). The role for the *dpp* pathway in preventing progenitor cell death we have discovered would, in principle, connect *ey* function to cell death. At present we do not have a mechanistic explanation for why eye progenitor cells are prone to die (a tendency akin to the "death by default" state of cells proposed by Raff (Raff, 1992)), or how *dpp* signaling prevents it, but these are very relevant questions worth pursuing.

Is this control mechanism, based on regulating the rate of cell death of proliferating progenitors, working beyond the eyes? Although not tested formally, the result from Neto-Silva and co-workers, showing that wing asymmetry increased dramatically in mutants for the apoptosis regulator *hid* (Neto-Silva et al., 2009), suggests that apoptosis regulation may be involved in the control of developmental stability also of wings too. Beyond *Drosophila,* developmental apoptosis is very frequent (Fuchs and Steller, 2011) and, in some cases, associated to the regulation of cell number, with the mammalian immune cells (Rathmel, 10.1111/j.0105-2896.2004.0096.x) and the nervous systems (Raff et al., 1993) being striking examples. Therefore, it seems very possible to us that mechanisms similar to the one we have described here will use the feedback modulation of apoptosis as a means not only to controlling organ size, but also size robustness in other developmental systems as well.

MATERIALS AND METHODS

RESOURCE AVAILABILITY

Lead contact: Further information and requests for resources and reagents should be directed to and will be fulfilled by the lead contacts, Fernando Casares (fcasfer@upo.es) and Saul Ares (saul.ares@csic.es).

Materials availability: this study did not generate new unique reagents.

Data and code availability: images (as .tiff flies) and quantifications of all genotypes analyzed that might be required to reanalyze the data reported in this paper are available from the lead contacts upon request. The macros for the quantification of apoptosis/proliferation signal from confocal images is provided as supplementary material. Any additional information required to reanalyze the data reported in this paper is available from the lead contacts upon request.

METHOD DETAILS

Drosophila strains and genetic manipulations

The *optix2/3-GAL4* driver (abbreviated "*optix>*") is expressed in undifferentiated eye progenitors (Neto et al., 2017). Other strains used were: *UAS-tkvRNAi* (VDRC #102319), *UAS-DadRNAi* (VDRC #108340), *UAS-Dad* (Tsuneizumi et al., 1997) and *UAS-RHGRNAi* (Siegrist et al., 2010). The *optix2/3-GAL4, UAS-tkvRNAi/CyO* recombinant strain was generated by standard genetic methods. Other strains used were the *dpp* transcriptional reporter *dpp-Z* (Masucci and Hoffmann, 1993), the *Bar* mutant on the FM7c balancer chromosome (Flybase: FBba0000009) and the wild type strain *Oregon-R (Or-R)*. The *UAS-mCherry* RNAi line (Bloomington stock centre, reference BDSC_35785) was used as a neutral UAS-RNAi line.

Immunofluorescence and confocal imaging:

Fixation and immunofluorescence of eye primordia was done as in (Neto et al., 2016). Imaging was carried out on a Leica SPE confocal setup. Images were then processed using ImageJ. Primary antibodies used were: rabbit *anti*-phospho-histone H3 (pH3) used at 1:1000 (Sigma), rabbit *anti*-Dcp 1 (Dcp-1) used at 1:200 (Cell Signaling Technology). Fluorescence secondary antibodies were from Molecular Probes and

439 used at 1:1000. Rhodamine-phalloidin used at 1:400 (Life technologies), was used in
440 some experiments to counterstain the tissue. All primary and secondary antibodies
441 were diluted in PBT (PBS + 0,1% Triton X-100).
442
443 QUANTIFICATION AND STATISTICAL ANALYSIS
444 **Quantification of adult eye size**
445 Heads of 1-3 day old adult males and females were dissected in PBS, cleared with
446 15% Hydrogen Peroxide and mounted in Hoyer's medium: lactic acid (1:1) (Casares
447 and Mann, 2000). Frontal and occipital planes of each head were photographed using
448 a 10X objective on a Leica DM5000B microscope and a Leica DFC490 digital
449 camera. The areas of the eyes and head were measured using the polygonal tool of
450 ImageJ (Rueden et al., 2017) and expressed as arbitrary units. The Supplementary
451 figure to Materials and Methods illustrates the areas as measured. The area of each
452 eye was obtained as the sum of the area of the eye in the frontal and occipital planes.
453 **Quantification of mitotic and apoptotic rates**
454 To quantify the apoptosis (detected with anti-Dcp-1) and mitosis (detected with anti-
455 PH3) rates as the Dcp-1/PH3 signal relative to the area anterior to the morphogenetic
456 furrow (i.e. differentiation wave front), we wrote a plug-in for ImageJ (included as
457 Supplementary material). Briefly, it works as follows: First, for each sample, the images
458 of a 3D confocal stack are projected along the Z-axis using the maximum pixel
459 intensity. Then, a Region of Interest (ROI) is drawn by hand to define the region of the
460 eye disc anterior to the morphogenetic furrow, which contains the undifferentiated eye
461 cells. A threshold for pixel intensity is chosen manually on the green channel (Dcp-
462 1/PH3), making sure that the thresholded area includes accurately all the signal. This
463 threshold level is kept for every sample of the series, which were acquired with exactly
464 the same microscope configuration. Finally, the thresholded area is projected onto the
465 original image for the Mean Intensity Value and Integrated Density to be measured.
466 **Statistical analysis**
467 The statistical analyses were supported on *Rsoftware* (R-Core-Team, 2013) and
468 hypothesis decisions were made under 95% confidence threshold in all cases.
469 **Modeling for intergroups comparison**
470 The metrics of interest were modeled depending on genoype group and sex factors by
471 fitting a median regression model (quantile regression: *rq* function from *quantreg* library
472 for factors) where normality and homoscedasticity assumptions are not required
473 (Howard, 2018). This model allows estimating the effect of the different covariables and
474 factors in the median of the response variable, thus allowing the prediction of the
475 median response variable for each group as a sum of the corresponding effects
476 (Beyerlein, 2014). In our context, the *optix>+* group was set as reference level and
477 genotype group was coded as multiple dummy factors of presence/absence of each
478 genotype. Thus, the effect of simultaneous downregulation of two genes is also
479 evaluated as an interaction term in the model. Models considering or not sex as factor
480 were compared by calculating F-statistic of the ratio of variances explained by each
481 fitted model (*anova* function). Sex effect turned out to be non-significant regardless of
482 the response variable evaluated, thus, the general model is denoted by the following
483 expression:
484

$$y_i = \beta_{0;0.5}(optix) + \beta_{1;0.5}\, RHGRI_i + \beta_{2;0.5}\, tkvRI_i + \beta_{3;0.5}\, tkvRI_i\, DadRI_i + \beta_{4;0.5}\, DadRI_i + \beta_{5;0.5}\, tkvRI_i\, RHGRI_i + \beta_{6;0.5}\, Bar_i + \beta_{7;0.5}\, Bar_i\, RHGRI_i + \beta_{8;0.5}\, Bar_i\, DadRI_i + u_{i,0.5}$$

where:

y_i is the i-th value of rE or %Apop variables;

$\beta_{j,0.5}$ is the j-th value of the estimated conditioned coefficient to the 0.5 quantile;

$u_{i,0.5}$ is the i-th value of the error variable conditioned to the 0.5 quantile.

Comparison of sFAi variances of each genotype versus control

The signed Fluctuation Asymmetry (sFAi) is a intraindividual measure of eye size precision. It is calculated as the relative differences between intraindividual (Left and Right) eye areas:

$$sFA_i = (L - R)/(L + R)$$

We compared intergroup sFAi through their variances since sFAi distributions are theoretically centered on 0. First, we assume there are no intragroup variance differences due to sex (Levene test median centered; *LeveneTest function* from *car* package). Second, median was subtracted for each group-sex combination to perform a sex-independent comparison. Finally, Levene test median centered was performed for pairwise comparisons of each group against the control one (*optix>+)*. P.values were adjusted by Benjamini-Hochberg method (*LeveneTest* function from *car* package and *p.adj* function*, method= "BH").*

Comparison of rE variances of each genotype versus control

rE variance is a interindividual measure of size precision in eye development. First, we assumed there were no intragroup variance differences due to sex (Levene test median centered; *LeveneTest function* from *car* package). Second, median was subtracted for each group-sex combination to perform a sex-independent comparison. Finally, Levene test median centered was performed for pairwise comparisons of each group against the control one (*optix>+)*. P.values were adjusted by Benjamini-Hochberg method (*LeveneTest* function from *car* package and *p.adj* function*, method= "BH").*

REFERENCES

Barrio, L., Milan, M., 2017. Boundary Dpp promotes growth of medial and lateral regions of the Drosophila wing. Elife 6.

Bessa, J., Gebelein, B., Pichaud, F., Casares, F., Mann, R.S., 2002. Combinatorial control of Drosophila eye development by eyeless, homothorax, and teashirt. Genes Dev 16, 2415-2427.

Beyerlein, A., 2014. Quantile Regression—Opportunities and Challenges From a User's Perspective. American Journal of Epidemiology 180, 330-331.

Blackman, R.K., Sanicola, M., Raftery, L.A., Gillevet, T., Gelbart, W.M., 1991. An extensive 3' cis-regulatory region directs the imaginal disk expression of decapentaplegic, a member of the TGF-beta family in Drosophila. Development 111, 657-666.

Bosch, P.S., Ziukaite, R., Alexandre, C., Basler, K., Vincent, J.P., 2017. Dpp controls growth and patterning in Drosophila wing precursors through distinct modes of action. Elife 6.

528 Boulan, L., Leopold, P., 2021. What determines organ size during development and
529 regeneration? Development 148.
530 Brummel, T.J., Twombly, V., Marques, G., Wrana, J.L., Newfeld, S.J., Attisano, L.,
531 Massague, J., O'Connor, M.B., Gelbart, W.M., 1994. Characterization and relationship
532 of Dpp receptors encoded by the saxophone and thick veins genes in Drosophila. Cell
533 78, 251-261.
534 Bryant, P.J., 1988. Localized cell death caused by mutations in a Drosophila gene
535 coding for a transforming growth factor-beta homolog. Dev Biol 128, 386-395.
536 Casares, F., Mann, R.S., 2000. A dual role for homothorax in inhibiting wing blade
537 development and specifying proximal wing identities in Drosophila. Development 127,
538 1499-1508.
539 Casares, F., McGregor, A.P., 2020. The evolution and development of eye size in flies.
540 Wiley interdisciplinary reviews. Developmental biology, e380.
541 Chanut, F., Heberlein, U., 1995. Role of the morphogenetic furrow in establishing
542 polarity in the Drosophila eye. Development 121, 4085-4094.
543 Chanut, F., Heberlein, U., 1997. Role of decapentaplegic in initiation and progression
544 of the morphogenetic furrow in the developing Drosophila retina. Development 124,
545 559-567.
546 Colombani, J., Andersen, D.S., Leopold, P., 2012. Secreted peptide Dilp8 coordinates
547 Drosophila tissue growth with developmental timing. Science 336, 582-585.
548 Fried, P., Sanchez-Aragon, M., Aguilar-Hidalgo, D., Lehtinen, B., Casares, F., Iber, D.,
549 2016. A Model of the Spatio-temporal Dynamics of Drosophila Eye Disc Development.
550 PLoS Comput Biol 12, e1005052.
551 Fuchs, Y., Steller, H., 2011. Programmed cell death in animal development and
552 disease. Cell 147, 742-758.
553 Garelli, A., Gontijo, A.M., Miguela, V., Caparros, E., Dominguez, M., 2012. Imaginal
554 discs secrete insulin-like peptide 8 to mediate plasticity of growth and maturation.
555 Science 336, 579-582.
556 Greenwood, S., Struhl, G., 1999. Progression of the morphogenetic furrow in the
557 Drosophila eye: the roles of Hedgehog, Decapentaplegic and the Raf pathway.
558 Development 126, 5795-5808.
559 Heberlein, U., Moses, K., 1995. Mechanisms of Drosophila retinal morphogenesis: the
560 virtues of being progressive. Cell 81, 987-990.
561 Heberlein, U., Wolff, T., Rubin, G.M., 1993. The TGF beta homolog dpp and the
562 segment polarity gene hedgehog are required for propagation of a morphogenetic
563 wave in the Drosophila retina. Cell 75, 913-926.
564 Howard, M., 2018. Comparison of the Performance of Simple Linear Regression and
565 Quantile Regression with Non-Normal Data: A simulation study, Mathematics.
566 University of South Carolina.
567 Hunt, D.M., 1971. The physiological control of gene action in the eyeless and eyegone
568 mutants of Drosophila melanogaster. Genet Res 17, 195-208.
569 Inoue, H., Imamura, T., Ishidou, Y., Takase, M., Udagawa, Y., Oka, Y., Tsuneizumi, K.,
570 Tabata, T., Miyazono, K., Kawabata, M., 1998. Interplay of signal mediators of
571 decapentaplegic (Dpp): molecular characterization of mothers against dpp, Medea, and
572 daughters against dpp. Mol Biol Cell 9, 2145-2156.
573 Kang, J., Yeom, E., Lim, J., Choi, K.W., 2014. Bar represses dPax2 and
574 decapentaplegic to regulate cell fate and morphogenetic cell death in Drosophila eye.
575 PLoS One 9, e88171.
576 Lander, A.D., 2011. Pattern, growth, and control. Cell 144, 955-969.
577 Lander, A.D., Gokoffski, K.K., Wan, F.Y., Nie, Q., Calof, A.L., 2009. Cell lineages and
578 the logic of proliferative control. PLoS Biol 7, e15.
579 Lee, J.J., von Kessler, D.P., Parks, S., Beachy, P.A., 1992. Secretion and localized
580 transcription suggest a role in positional signaling for products of the segmentation
581 gene hedgehog. Cell 71, 33-50.

582 Lobo-Cabrera, F.J., Navarro, T., Iannini, A., Casares, F., Cuetos, A., 2021. Quantitative
583 Relationships Between Growth, Differentiation, and Shape That Control Drosophila
584 Eye Development and Its Variation. Front Cell Dev Biol 9, 681933.
585 Lopes, C.S., Casares, F., 2010. hth maintains the pool of eye progenitors and its
586 downregulation by Dpp and Hh couples retinal fate acquisition with cell cycle exit. Dev
587 Biol 339, 78-88.
588 Ma, C., Zhou, Y., Beachy, P.A., Moses, K., 1993. The segment polarity gene hedgehog
589 is required for progression of the morphogenetic furrow in the developing Drosophila
590 eye. Cell 75, 927-938.
591 Masucci, J.D., Hoffmann, F.M., 1993. Identification of two regions from the Drosophila
592 decapentaplegic gene required for embryonic midgut development and larval viability.
593 Dev Biol 159, 276-287.
594 Masucci, J.D., Miltenberger, R.J., Hoffmann, F.M., 1990. Pattern-specific expression of
595 the Drosophila decapentaplegic gene in imaginal disks is regulated by 3' cis-regulatory
596 elements. Genes Dev 4, 2011-2023.
597 Matsuda, S., Affolter, M., 2017. Dpp from the anterior stripe of cells is crucial for the
598 growth of the Drosophila wing disc. Elife 6.
599 Morgante, F., Sorensen, P., Sorensen, D.A., Maltecca, C., Mackay, T.F., 2015. Genetic
600 Architecture of Micro-Environmental Plasticity in Drosophila melanogaster. Scientific
601 reports 5, 9785.
602 Neto, M., Aguilar-Hidalgo, D., Casares, F., 2016. Increased avidity for Dpp/BMP2
603 maintains the proliferation of progenitors-like cells in the Drosophila eye. Dev Biol 418,
604 98-107.
605 Neto, M., Naval-Sanchez, M., Potier, D., Pereira, P.S., Geerts, D., Aerts, S., Casares,
606 F., 2017. Nuclear receptors connect progenitor transcription factors to cell cycle
607 control. Scientific reports 7, 4845.
608 Neto-Silva, R.M., Wells, B.S., Johnston, L.A., 2009. Mechanisms of growth and
609 homeostasis in the Drosophila wing. Annu Rev Cell Dev Biol 25, 197-220.
610 Neumann, C.J., Nuesslein-Volhard, C., 2000. Patterning of the zebrafish retina by a
611 wave of sonic hedgehog activity. Science 289, 2137-2139.
612 Niven, J.E., Laughlin, S.B., 2008. Energy limitation as a selective pressure on the
613 evolution of sensory systems. J Exp Biol 211, 1792-1804.
614 Parsons, P.A., 1992. Fluctuating asymmetry: a biological monitor of environmental and
615 genomic stress. Heredity (Edinb) 68 (Pt 4), 361-364.
616 R-Core-Team, 2013. R: A language and environment for statistical computing. R
617 Foundation for Statistical Computing, Vienna, Austria.
618 Raff, M.C., 1992. Social controls on cell survival and cell death. Nature 356, 397-400.
619 Raff, M.C., Barres, B.A., Burne, J.F., Coles, H.S., Ishizaki, Y., Jacobson, M.D., 1993.
620 Programmed cell death and the control of cell survival: lessons from the nervous
621 system. Science 262, 695-700.
622 Rogers, E.M., Brennan, C.A., Mortimer, N.T., Cook, S., Morris, A.R., Moses, K., 2005.
623 Pointed regulates an eye-specific transcriptional enhancer in the Drosophila hedgehog
624 gene, which is required for the movement of the morphogenetic furrow. Development
625 132, 4833-4843.
626 Roignant, J.Y., Treisman, J.E., 2009. Pattern formation in the Drosophila eye disc. Int J
627 Dev Biol 53, 795-804.
628 Rueden, C.T., Schindelin, J., Hiner, M.C., DeZonia, B.E., Walter, A.E., Arena, E.T.,
629 Eliceiri, K.W., 2017. ImageJ2: ImageJ for the next generation of scientific image data.
630 BMC Bioinformatics 18, 529.
631 Siegrist, S.E., Haque, N.S., Chen, C.H., Hay, B.A., Hariharan, I.K., 2010. Inactivation of
632 both Foxo and reaper promotes long-term adult neurogenesis in Drosophila. Curr Biol
633 20, 643-648.
634 Song, Z., McCall, K., Steller, H., 1997. DCP-1, a Drosophila cell death protease
635 essential for development. Science 275, 536-540.

636 Spencer, F.A., Hoffmann, F.M., Gelbart, W.M., 1982. Decapentaplegic: a gene
637 complex affecting morphogenesis in Drosophila melanogaster. Cell 28, 451-461.
638 Tice, S.C., 1914. A new sex-linked character in Drosophila. Biol. Bull. 26, 221-230.
639 Tsuneizumi, K., Nakayama, T., Kamoshida, Y., Kornberg, T.B., Christian, J.L., Tabata,
640 T., 1997. Daughters against dpp modulates dpp organizing activity in Drosophila wing
641 development. Nature 389, 627-631.
642 Vollmer, J., Fried, P., Aguilar-Hidalgo, D., Sanchez-Aragon, M., Iannini, A., Casares,
643 F., Iber, D., 2017. Growth control in the Drosophila eye disc by the cytokine Unpaired.
644 Development 144, 837-843.
645 Vollmer, J., Fried, P., Sanchez-Aragon, M., Lopes, C.S., Casares, F., Iber, D., 2016. A
646 quantitative analysis of growth control in the Drosophila eye disc. Development 143,
647 1482-1490.
648 Waddington, C.H., 1942. Canalization of development and the inheritance of acquired
649 characters. Nature 150, 563–565.
650 Wartlick, O., Julicher, F., Gonzalez-Gaitan, M., 2014. Growth control by a moving
651 morphogen gradient during Drosophila eye development. Development 141, 1884-
652 1893.
653 Weasner, B.M., Kumar, J.P., 2022. The timing of cell fate decisions is crucial for
654 initiating pattern formation in the Drosophila eye. Development 149.
655 Wolpert, L., 2010. Arms and the man: the problem of symmetric growth. PLoS Biol 8.
656 Zhu, J., Palliyil, S., Ran, C., Kumar, J.P., 2017. Drosophila Pax6 promotes
657 development of the entire eye-antennal disc, thereby ensuring proper adult head
658 formation. Proc Natl Acad Sci U S A 114, 5846-5853.
659